

## Article

# Hydrodynamic Performance Study of a Reciprocating Plate Column Driven by Electro-permanent Magnet Technology

Kai Guo <sup>1</sup>, Jianxu Jiang <sup>1</sup>, Deqiang Zhang <sup>1</sup>, Linyuan Meng <sup>1</sup>, Yiran Zhang <sup>1</sup>, Xiantao Fan <sup>2,\*</sup> and Hongsheng Zhang <sup>1,\*</sup>

<sup>1</sup> Hebei Key Laboratory of Heavy Metal Deep-Remediation in Water and Resource Reuse, School of Environment and Chemical Engineering, Yanshan University, Qinhuangdao 066004, China; kguo@ysu.edu.cn (K.G.); jjx19990204@163.com (J.J.); 18245305881@163.com (D.Z.); mlyysu@126.com (L.M.); 13383355660@163.com (Y.Z.)

<sup>2</sup> Department of Aerospace and Mechanical Engineering, University of Notre Dame, Notre Dame, IN 46556, USA

\* Correspondence: xfan2@nd.edu (X.F.); zhsysu@126.com (H.Z.)

**Abstract:** The reciprocating plate column is a kind of column with the plates driven by a geared motor, and it has advantages in regard to efficiency compared to traditional columns in the extraction process, however, it comes with an increase in energy consumption. A new type of reciprocating plate column driven by electro-permanent magnet technology (EPM) is proposed in this paper to obtain a better performance with lower energy consumption. The feasibility and performance of the proposed column is studied by numerical simulation and experiments with a kerosene–water system. The electro-permanent magnet chuck could provide a maximum amplitude of 12 mm in this study. Kerosene was used as the dispersed phase, and deionized water was used as the continuous phase, in a laboratory-scale 35 mm diameter reciprocating plate column driven by EPM. Hydrodynamic performance experiments were carried out with different flowrates of both phases and reciprocating frequencies. The experimental results show that the electro-permanent magnet chuck, which serves as the driving device of the reciprocating plate column, plays the role of adding energy and increasing the droplet breakage. In addition, the energy consumption of the reciprocating plate column with traditional geared motor and electro-permanent magnet chuck is calculated respectively. Compared with the traditional geared motor, the energy saving of the electro-permanent magnet chuck is as high as 98.55%.

**Keywords:** reciprocating plate column; electro-permanent magnet; fluid dynamic; energy analysis



**Citation:** Guo, K.; Jiang, J.; Zhang, D.; Meng, L.; Zhang, Y.; Fan, X.; Zhang, H. Hydrodynamic Performance Study of a Reciprocating Plate Column Driven by Electro-permanent Magnet Technology. *Machines* **2024**, *12*, 330. <https://doi.org/10.3390/machines12050330>

Academic Editors: Antonios Gasteratos and Theoklitos Karakatsanis

Received: 15 April 2024

Revised: 8 May 2024

Accepted: 10 May 2024

Published: 13 May 2024



**Copyright:** © 2024 by the authors. Licensee MDPI, Basel, Switzerland. This article is an open access article distributed under the terms and conditions of the Creative Commons Attribution (CC BY) license (<https://creativecommons.org/licenses/by/4.0/>).

## 1. Introduction

Solvent extraction is a vital chemical separation technology widely that is used in the pharmaceuticals industry [1], petrochemical engineering, hydrometallurgy, etc. [2]. Traditional extraction equipment includes the mixing tank, spray tower, packed tower, and sieve plate tower [3,4]. The extraction column has advantages of a good sealing, compact structure, high volumetric efficiency, and reliable performance [4,5]. However, the mass transfer efficiency of extraction column is limited and is hard to improve without external stirring.

In order to solve this problem, Van Dijk [6] proposed an extraction column by pulsing the fluid in the column or reciprocating the sieve plate to improve the mass transfer efficiency. Subsequently, Karr [7] developed a reciprocating sieve plate column, which periodically moves up and down through the sieve plate to break droplets and increase the mass transfer efficiency. The Karr reciprocating plate column has the advantages of a high mass transfer efficiency, large flux, and low axial mixing, and it has been widely used in pharmaceutical, petrochemical, metallurgical, and other industries [8], especially in the purification of pharmaceutical compounds [9].

Many scholars have studied the fluid dynamics performance of Karr columns [10]. Baird et al. studied the drop diameter and dispersed phase holdup in a column without mass transfer [11]. The experiment showed that the drop diameter is usually not affected by throughput but depends on the vibration intensity of the sieve plate and the properties of the system. Parthasarathy et al. considered the influence of the free area of the plate, plate spacing, and continuous phase velocity on the residence time of continuous phase based on the influence of sieve plate vibration intensity and dispersed phase velocity on the residence time of continuous phase in the column [12]. Bensalem. A et al. studied the drop diameter and drop size distribution in a system with and without mass transfer [13]. Experiments have shown that vibration has a significant impact on the diameter and distribution of drop, and correlations for drop diameter have been proposed under conditions of mass transfer and no mass transfer, respectively.

Reducing energy consumption is very important for reciprocating a plate column, which needs extra energy input. The American Walker Company [14] first designed and produced the electromagnetic chuck, which is considered to be the prototype of the electro-permanent magnet chuck. With the development of permanent magnetic materials, AlNiCo permanent magnetic materials with low coercivity and high remanence [15] came out, and the French Braillon Magnetics company [16] invented the unloadable permanent magnet chuck in the 1930s, using this material. The Italian company TECNOMAGNETE successfully used the magnetic difference principle to manufacture an electro-permanent magnet chuck [17]. TECNOMAGNETE's electro-permanent magnet chuck uses an electric pulse control method. The modern electro-permanent magnet chuck has the advantages of strong suction, low energy consumption, less heat, no loss of magnetism, a small size, and a light weight [18].

Recently, the electro-permanent magnet technology has gained applications in many aspects. Qin's group [19] applied the electro-permanent magnet chuck to the drawing process and designed a magnetic blank-holder device, which greatly simplified the blank-holder structure. Chang Pei [20] of Ningbo University applied the electro-permanent magnet chuck technology to the shipbuilding industry and designed and developed a new type of ship mooring device based on the electro-permanent magnet chuck. Based on the electro-permanent magnet technology, Chang Xu et al. [21]. of Tsinghua University innovatively applied the electronically controlled permanent magnet chuck to the horizontal well tractors. The working state of the sucker is controlled by the pulse current, and the working capacity of the chuck is provided by the permanent magnet material. With the continuous advancement of technology, the performance of electronically controlled permanent magnet suckers has also been further improved. The driving force of the reciprocating plate column based on the electro-permanent magnet technology is provided by the electro-permanent magnet technology chuck. The above studies provide favorable references for our device.

In this work, a new type of reciprocating plate column based on electro-permanent magnet technology was proposed to realize higher efficiency and energy conversation. The feasibility of this new type of reciprocating plate column was verified via experiments. The hydrodynamic performance experiments were carried out using this equipment, including the study of the Sauter mean drop size and the study of the dispersed phase holdup. Finally, the energy consumption analysis of the vibrating sieve plate tower based on the electronically controlled permanent magnet technology proves that it has great advantages in energy saving.

## 2. Materials and Methods

### 2.1. Design of EPM Reciprocating Plate Column

A laboratory-scale reciprocating plate column based on EPM technology was established in this study, and the schematic diagram of the device is shown in Figure 1. The main body of the tower is made of glass, and both the top and bottom of the columns have expanded areas which were used as buffer zones for the organic and aqueous phases, respectively. The organic phase pump and the water phase pump are set at the bottom

of the column: and the organic phase outlet is set at the top of the column, and the water phase outlet is set at the bottom of the column. The two-phase system used in this experiment consists of kerosene and water. Since tap water contains many impurities, deionized water [22] was used as the continuous phase. At the same time, aviation kerosene with high purity was selected as the dispersed phase. The kerosene in the organic phase water tank is pumped into the column by the organic phase pump from the bottom of the column through the organic phase inlet, and the deionized water in the water phase water tank is pumped into the column by the water phase pump through the water phase inlet at the top of the column. The density difference between the two phases is used to make the kerosene enter the product water tank from the top outlet of the column, and the deionized water returns to the water phase water tank through the  $\pi$ -type tube from the bottom outlet of the column. A stack of perforated plates made of stainless steel filled the center of the column, which was reciprocated using the electro-permanent magnet chuck installed at the top of the column. The reciprocating frequency of vibration is controlled by IPC. The specifications of the reciprocating plate column based on EPM technology and physical properties of the solvent system are given in Table 1.

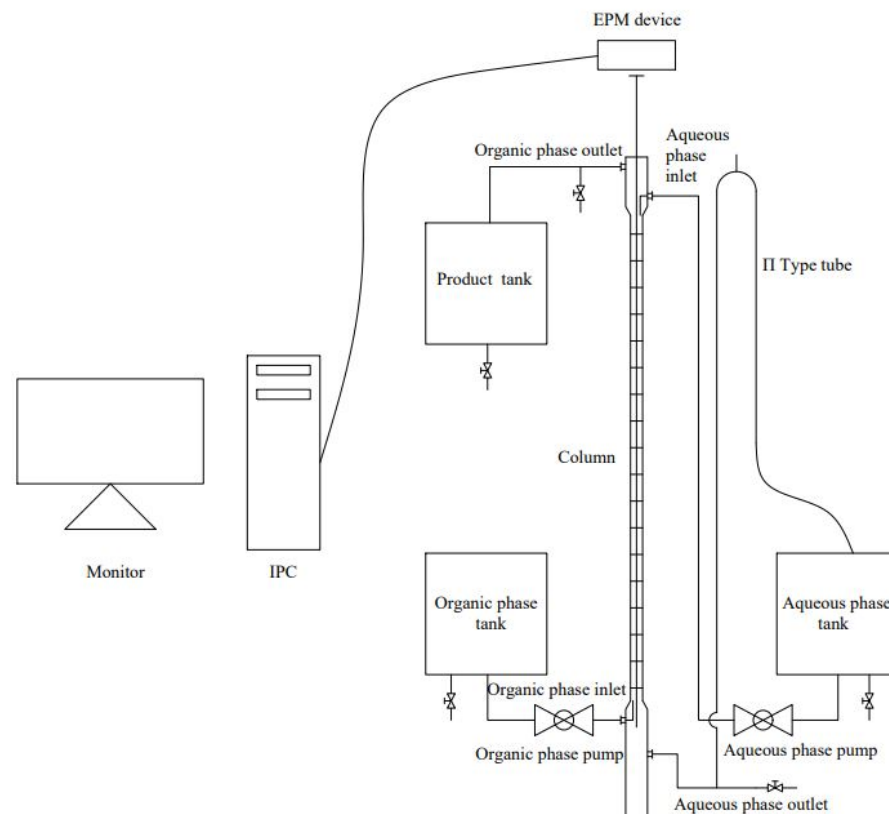


**Figure 1.** The schematic diagram of reciprocating plate column based on EPM technology.

Before the experiment, as shown in Figure 1, the organic phase is loaded with kerosene, and the water phase is loaded with deionized water. Referring to the previous scholars' experiments, the range of  $u_c$  and  $u_d$  is 10~70 mm/s, and four different frequencies of vibration are used for the experiment [23]. The experiment was designed as a 4 (dispersed phase velocity)  $\times$  4 (continuous phase velocity)  $\times$  4 (reciprocating frequency), which resulted in a total of 64 fluid dynamic experiments. The experimental design matrix is given in Table 2. The flow meters for both aqueous phase and organic phase were calibrated before the experiment.

**Table 1.** Specifications of the reciprocating plate column based on EPM technology.

| Name                       | Symbol   | Column                     |
|----------------------------|----------|----------------------------|
| Column diameter            | $D_c$    | 35 mm                      |
| Effective column height    | $H_c$    | 1 m                        |
| Number of plates           | $N$      | 18                         |
| Plate thickness            | $E$      | 1.5 mm                     |
| Plate material             | -        | Stainless steel            |
| Perforation diameter       | $d_h$    | 2 mm                       |
| Plate spacing              | $h_c$    | 50 mm                      |
| Amplitude                  | $A$      | 10 mm                      |
| Dispersed phase            | $d$      | kerosene                   |
| Continuous phase           | $c$      | deionized water            |
| Dispersed phase density    | $\rho_d$ | 775 kg/m <sup>3</sup>      |
| Continuous phase density   | $\rho_c$ | 1000 kg/m <sup>3</sup>     |
| Dispersed phase viscosity  | $\mu_c$  | $2.21 \times 10^{-3}$ Pa·s |
| Continuous phase viscosity | $\mu_d$  | $8.94 \times 10^{-4}$ Pa·s |

**Table 2.** Experimental design matrix.

| Continuous Phase Velocity,<br>$v_c$ (L/h) | Dispersed Phase Velocity, $v_d$<br>(L/h) | Reciprocating Frequency,<br>$f$ (times/min) |
|---|--|---|
| 2   | 6  | 0   |
| 4   | 9  | 2   |
| 6   | 12                                       | 4   |
| 8   | 15                                       | 6   |

## 2.2. Materials

This study investigated the hydrodynamic characteristics of EPM-RPC in a two-phase flow system of water–kerosene without mass transfer. Water enters as a continuous phase from the top of the column, while kerosene enters as a dispersed phase from the bottom of the column. The two-phase flow velocity is adjusted by a rotameter installed on the water and kerosene inlet pipeline and then calibrated by the flowmeter. The continuous phase flow velocity ( $u_c$ ) range is 7.08–28.3 mm/s, and the dispersed phase flow velocity ( $u_d$ ) is 10.3–44.28 mm/s; the experimental operating condition is kept away from the flooding point of the column. The study also measured the basic physical properties of continuous and dispersed phases, including the density, viscosity, and interfacial tension, in the laboratory. The measurement results are shown in Table 3.

**Table 3.** Physical properties of the test system at 25 °C, 1 atm.

| Phase            | Material | Density (kg/m <sup>3</sup> ) | Viscosity (mPa·s) | Interfacial Tension (mN/m) |
|------------------|----------|------------------------------|-------------------|----------------------------|
| Continuous phase | Water    | 998.20                       | 1.06              | 22                         |
| Dispersed phase  | Kerosene | 810.25                       | 2.10              |                            |

## 2.3. Design of Reciprocating Device

The driving mode of the traditional reciprocating plate column is shown in Figure 2a. The driving force is generated by the rotation of the geared motor, and the torque is transmitted by the eccentric wheel mechanism, which drives the joint bearing with the rod end and the central shaft to move up and down. The sieve plates are fixed on the central shaft and move periodically with the rotation of the motor.

The drive mode of the reciprocating plate column based on EPM technology is shown in Figure 2b, where the sieve plates are fixed on the central shaft, and the central shaft is connected to the suction part by thread. The electro-permanent magnet chuck enters the magnetization state, generating a large enough suction force to make the suction part

and the fixed sieve plate below have an upward displacement. After completing this process, the electro-permanent magnet enters the demagnetization state, and the external performance is non-magnetic suction. Under the action of gravity, the suction part and the sieve plate complete the downward process. The magnetization and demagnetization state of the electro-permanent magnet chuck is completed as a cycle, which plays the same role in improving the mass transfer efficiency as the reciprocating plate column driven by the traditional geared motor.

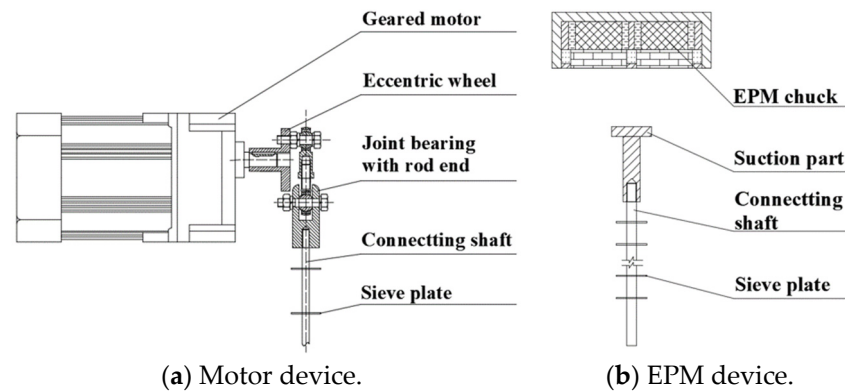


**Figure 2.** Driving mode of reciprocating plate column.

Figure 3 shows a pair of magnetic pole units designed based on the electro-permanent magnet technology. In the electro-permanent magnet technology, the magnetic pole units always work in pairs. The main body of the magnetic pole unit is permanent magnet Nb-Fe-B 2 with strong magnetism at Curie temperature, reversible magnet Al-Ni-Co 4 with low coercivity and high remanence, pure iron 3 with magnetic conductivity, and a coil used to change the direction and size of the magnetic field of the reversible magnet Al-Ni-Co. As shown in Figure 3a, in the magnetizing state, the magnetic field generated by the reversible magnet Al-Ni-Co is consistent with that of the permanent magnet Nb-Fe-B, and the magnetic field line passes through the suction plate to generate a strong magnetic attraction. As shown in Figure 3b, in the demagnetization state, the magnetic field generated by the reversible magnet Al-Ni-Co is opposite to that of the permanent magnet Nb-Fe-B. The magnetic field line completes the cycle inside and does not pass through the suction plate, showing no magnetic attraction to the outside.

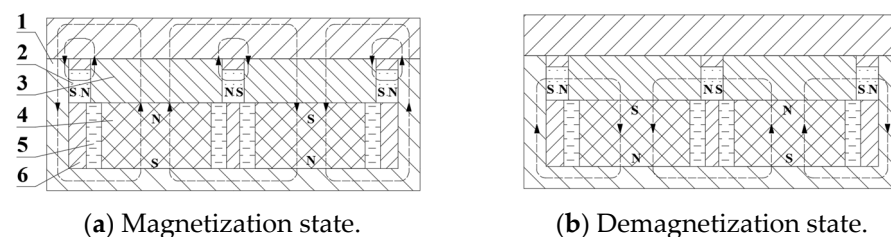


**Figure 3.** Magnetic pole units in magnetization and demagnetization states: (1) base, (2) PM, (3) magnetic conductor, (4) RM, (5) coil, and (6) epoxy resin.

In order to verify the magnetic attraction of the designed electro-permanent magnet reciprocating plate column drive device, Maxwell software is used to analyze the magnetic field of the electric control permanent magnet drive device. In the analysis, the thread of the suction part is simplified. The material properties used are shown in Table 4.

In order to verify the size of the magnetic force of the electro-permanent magnet reciprocating plate column designed in this paper under different amplitudes, the simulation was carried out with three different currents. The magnetic induction intensity cloud diagram is shown in Figure 4. It can be seen from Figure 5 that the magnetic suction force is the largest when the electric permanent magnet sucker is fitted with the suction part, and

the magnetic suction force decreases rapidly with the increase in the amplitude. When the amplitude is 12 mm, the magnetic suction is 19.45 N, and the current is 17 A. According to the design of the internals of the reciprocating plate column, the mass of the column's internals and the total mass of the suction parts are both about 1.1 kg. Therefore, in the designed reciprocating plate column based on the electro-permanent magnet technology, the amplitude can reach 12 mm, which is close to the amplitude of other reciprocating plate columns using geared motors 22.

**Table 4.** Material properties for magnetic field analysis.

| Materials    | Properties            |                               |                   |
|--------------|-----------------------|-------------------------------|-------------------|
|              | Relative Permeability | Bulk Conductivity (Siemens/m) | Coercivity (kA/m) |
| AlNiCo5      | B-H curve             | $2.128 \times 10^6$           | 52.5              |
| NbFeB        | 1.10                  | $6.25 \times 10^5$            | 928               |
| Pure iron    | 4000                  | $1.03 \times 10^7$            | 0                 |
| Carbon steel | 9000                  | $2.00 \times 10^6$            | 0                 |
| Air          | 1                     | /                             | /                 |
| Epoxy resin  | 1                     | /                             | /                 |

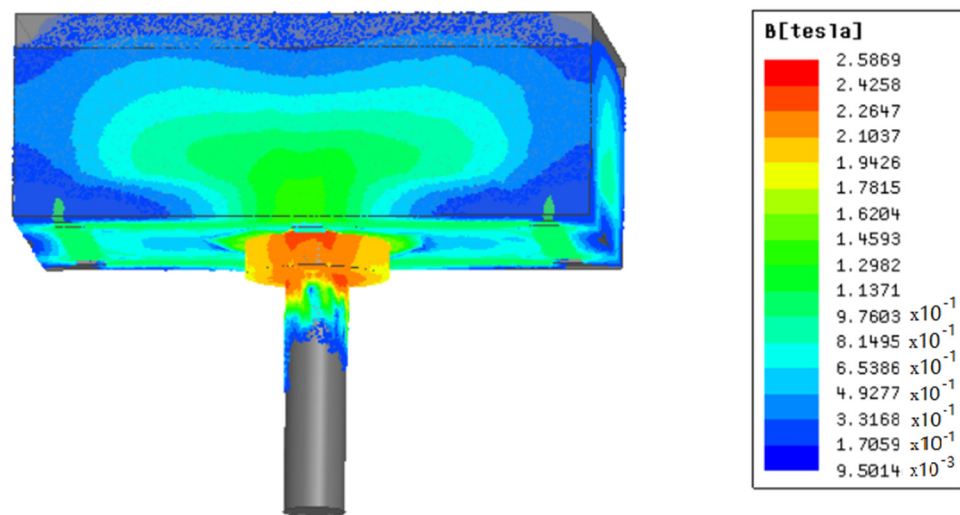


**Figure 4.** Electromagnetic simulation cloud map.

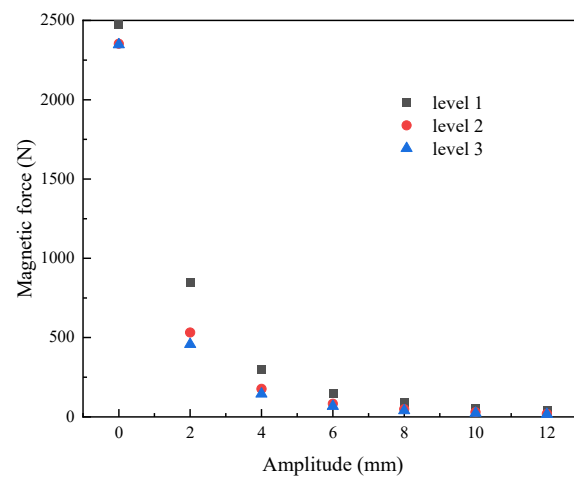


**Figure 5.** Relationship between amplitude and magnetic force.

## 2.4. Measurement and Data Processing

### (a) Drop size

The average droplet diameter of the dispersed phase is of great significance in the extraction tower. It not only affects the specific surface area that can be used for mass transfer; it also affects the mass transfer coefficient, flooding conditions, and dispersed phase retention rate. At the same time, because the movement of the droplets in the extraction tower is complex and the diameter distribution of the droplets is uneven, the average diameter of the dispersed phase droplets is usually used to represent the diameter of the droplets. The most commonly used is the average diameter of the Sauter dispersed phase droplets,  $d_{32}$ , to represent the average droplet diameter of the dispersed phase. The average diameter of the dispersed droplets,  $d_{32}$ , is defined as the ratio of the total droplet volume to the total droplet surface area, as shown in Equation (1):

$$d_{32} = \frac{\sum_{i=1}^n n_i d_i^3}{\sum_{i=1}^n n_i d_i^2} \quad (1)$$

where  $n_i$  is the number of droplets with a diameter of  $d_i$ .

For elliptical droplets, the lengths of the long axis and the short axis are measured and averaged. There are two methods for measuring the average droplet diameter,  $d_{32}$ , of the dispersed phase: direct method and indirect method.

The direct method is to directly measure the diameter of the dispersed phase droplets in the extraction equipment, and the field measurement has contact and non-contact methods. The contact method is to measure the local droplet diameter distribution by extending the sensor probe into the flow field of the extraction equipment. The non-contact method is to use camera equipment to capture the instantaneous flow field and then obtain the droplet diameter distribution through photo processing. The measurement method of the droplet diameter usually adopts non-contact. The specific process is to obtain the frequency histogram of droplet diameter distribution by a droplet image processing system after camera shooting when the two-phase flow of extraction equipment is stable, and then  $d_{32}$  is obtained by mathematical statistics. The indirect method is to calculate the average diameter of dispersed phase droplets by measuring other parameters of the two-phase flow in the extraction tower. There are chemical methods, light absorption methods, and other test methods, but the accuracy of the indirect method is low, so it is not commonly used. In this work, the non-contact method was adopted to obtain the diameter of the droplets.

### (b) Dispersed phase holdup

The definition of the dispersed phase liquid holdup is the ratio of the volume of the dispersed phase in the device to the effective operating volume. The significance of the dispersed phase retention fraction is that it reflects the proportion of the dispersed phase in the effective mass transfer area of the two phases, and the dispersed phase retention fraction and the average diameter of the dispersed droplets directly determine the mass transfer specific surface area of the two-phase fluid, indicating the mass transfer effect of the extraction. At the same time, the combination of the dispersed phase retention fraction and the two-phase apparent velocity can be directly fitted to calculate the characteristic velocity. Therefore, the dispersed phase liquid holdup is of great significance to the study of fluid mechanics of extraction equipment.

The determination methods of the dispersed phase liquid holdup mainly include the volume replacement method, differential pressure method, and mixed density method. Among them, the most commonly used method is the volume replacement method, which measures the height of the condensed layer before and after closing the inlet and outlet valves, and then calculates the retention fraction of the dispersed phase. This method is more accurate, but the operation is more cumbersome. The pressure difference method is based on static equilibrium calculation, which is simple and convenient, but the error is large. The mixing density method uses Y-rays or ultrasonic waves to measure the local

average density, thereby obtaining the local dispersed phase retention fraction. In this way, when the average diameter of the dispersed phase droplets ( $d_{32}$ ) and the dispersed phase liquid holdup are obtained in the experimental study, the mass transfer specific surface area of the droplet group in the unit tower volume can be calculated according to Equation (2). The mass transfer specific surface area is an important parameter, as it can be used to estimate the two-phase mass transfer in the extraction equipment and calculate the number of mass transfer units.

$$a = \frac{6\phi}{d_{32}} \quad (2)$$

(c) Axial mixing

When the fluid flows in the tower, due to the phenomenon of circulating flow and small eddy current, the fluid flow deviates from the ideal piston flow model. When the incompatible two-phase flow is reversed in the tower, vortex and phase entrainment may occur, which makes the velocity distribution inside the phase uneven. One part of the liquid velocity is greater than the average velocity, causing forward mixing, and the other part of the liquid velocity is lower than the average velocity, causing back mixing. Therefore, there is a big difference between the two-phase flow and the ideal piston flow, which is neither a plunger flow nor a completely mixed flow. The existence of axial mixing makes the mass transfer driving force and processing capacity decrease. For some large industrial extraction columns, the fluid flow in the tower deviates seriously from the ideal flow, and 60% to 75% of the column height is used to compensate for the loss of the mass transfer driving force caused by axial mixing. If the influence of axial mixing is not considered, the design and amplification of the extraction column is very difficult.

The fluid flow in the extraction tower is complex. There are many factors affecting the ideal flow of fluid, and it is very difficult to study its mechanism. Therefore, the mathematical model method is used to deal with the problem, and all the factors affecting the ideal flow in each phase are added and replaced by a model parameter. This parameter is the axial mixing coefficient, and its value can be disturbed by the tracer method, disturbance-response method, concentration method, profile method, and other methods of measurement.

In this study, the axial mixing coefficient was measured by the pulse tracer method. When the reciprocating plate column runs stably under the specified operating conditions, a certain amount of  $M_0$  saturated potassium chloride (KCl) solution is injected instantaneously into the tracer injection port of the continuous phase feed tube, the water phase sampling port is sampled at equal time intervals, and the conductivity is measured until the conductivity is stable. At the end of the experiment, the axial mixing coefficient can be calculated by the following steps.

In a certain concentration range, there is a linear relationship between the concentration of KCl aqueous solution and the conductivity, and the expression is as follows:

$$c_t - c_0 = K(k_t - k_0) \quad (3)$$

where  $c_0$  and  $k_0$  are the concentration and conductivity of the sample at  $t = 0$ ; that is, the concentration and conductivity of deionized water,  $c_t$  and  $k_t$ , are the concentration and conductivity of the sample at  $t$ .

When the initial time is  $t = 0$ , the concentration of KCl in deionized water is  $c = 0$ , so for  $c_t$ , the expression is as follows.

$$c_t = K(k_t - k_0) \quad (4)$$

Since the experimental process is equal time interval  $\Delta t$  sampling detection, according to the tracer inlet and outlet conservation during the experiment, the tracer injection amount,  $M_0$ , is approximately calculated as follows:

$$M_0 = \sum Q_c \cdot \Delta t \cdot c_t = K Q_c \Delta t \sum (k_t - k_0) \quad (5)$$

For the pulse tracer method, the residence time distribution density,  $E(t)$ , is calculated as follows:

$$E(t) = \frac{Q_c}{M_0} c_t = \frac{Q_c}{K Q_c \Delta t \sum (k_t - k_0)} \cdot K (k_t - k_0) = \frac{1}{\Delta t} \frac{k_t - k_0}{\sum (k_t - k_0)} \quad (6)$$

Therefore, the dimensionless variance ( $\delta^2$ ) expression can be obtained as shown in Equation (7):

$$\delta^2 = \frac{\delta_t^2}{\hat{t}^2} \quad (7)$$

The mathematical expectation,  $\hat{t}$ , can be obtained as shown in Equation (8), and the variance,  $\delta_t^2$ , can be obtained as shown in Equation (9).

$$\hat{t} = \frac{\sum t E(t)}{\sum E(t)} = \frac{\sum t \frac{1}{\Delta t} \frac{k_t - k_0}{\sum (k_t - k_0)}}{\sum \frac{1}{\Delta t} \frac{k_t - k_0}{\sum (k_t - k_0)}} = \frac{\sum t (k_t - k_0)}{\sum (k_t - k_0)} \quad (8)$$

$$\delta_t^2 = \frac{\sum t^2 E(t)}{\sum E(t)} - \hat{t}^2 = \frac{\sum t^2 \frac{1}{\Delta t} \frac{k_t - k_0}{\sum (k_t - k_0)}}{\sum \frac{1}{\Delta t} \frac{k_t - k_0}{\sum (k_t - k_0)}} - \hat{t}^2 = \frac{\sum t^2 (k_t - k_0)}{\sum (k_t - k_0)} - \hat{t}^2 \quad (9)$$

In this study, the injection port of the tracer KCl is at the feed pipe, the flow of the continuous phase in the inlet pipe is plug flow ( $Re < 2000$ ), and the outlet detection is at the sampling port of the aqueous phase of the extraction tower. This detection device is an 'open-closed' container device, so the continuous phase Peclet number,  $Pe$ , has the following relationship with the dimensionless variance,  $\delta^2$ :

$$Pe_c = \frac{3}{\sqrt{3\delta^2 + 1} - 1} \quad (10)$$

Then, the axial mixing coefficient,  $E_c$ , of the continuous phase is expressed as follows.

$$E_c = \frac{u_c l}{Pe_c} \quad (11)$$

It can be seen from the above mathematical derivation that the theoretical values of the mathematical  $\hat{t}$ , variance ( $\delta_t^2$ ), and dimensionless variance ( $\delta^2$ ) are related to the speed of conductivity change,  $K$ ,  $Q_c$ ,  $M_0$ , etc. The axial mixing coefficient,  $E_c$ , also has nothing to do with  $K$ ,  $M_0$ , etc. Therefore, the experiment does not need to determine the expression of the tracer KCl concentration and its conductivity, and it does not need to record the exact  $M_0$  value of the molar amount of the injected tracer.

### 3. Results

In the experiments, the reciprocating amplitude was set to 10 mm, and different dispersed phases, continuous phase flows, and vibration frequencies were used to investigate the detail properties of the fluid field.

#### 3.1. Drop Size

##### 3.1.1. Effect of Dispersed Flow Velocity

As is shown in Figure 6, without the reciprocating motion of the plate, the droplet diameter is generally larger. When reciprocating, the Sauter average droplet diameter,  $d_{32}$ , decreases significantly due to the input of external mechanical energy, so that the droplets are more easily destroyed. In addition, the dispersed phase enters the column from the bottom, rises along the gap between the column wall and the sieve plate, and converges

below some sieve plates, which is another reason for the resulting larger droplet diameter, as shown in Figure 7.

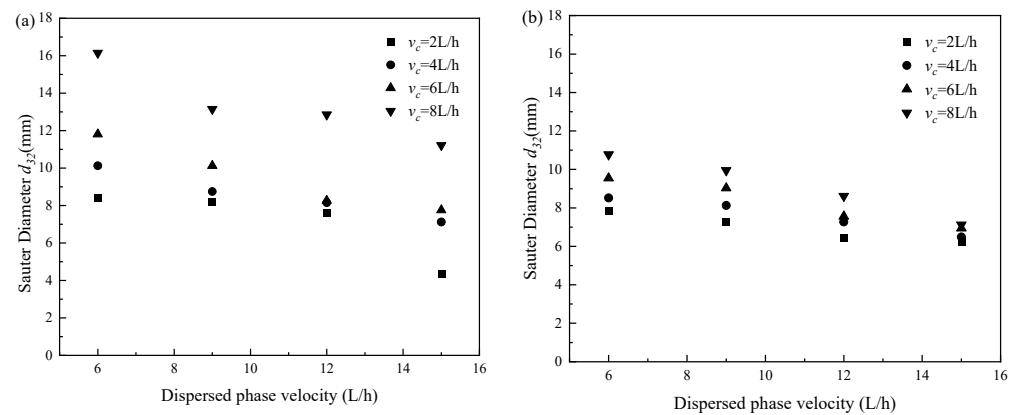


**Figure 6.** The droplet diameter: (a) stable and (b) reciprocating.

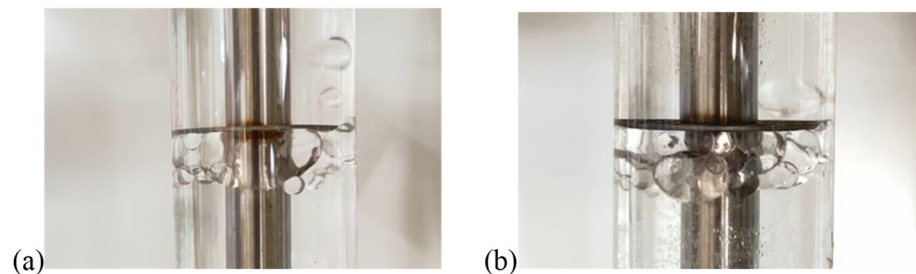


**Figure 7.** Drop size distribution: (a) stable and (b) reciprocating.

The Sauter average droplet diameter,  $d_{32}$ , decreases with the increase in the flow rate dispersed phase velocity,  $v_d$ . When the dispersed phase flow rate,  $v_d$ , is constant, the average  $d_{32}$  increases with the increase in the continuous phase flow rate  $v_c$ . The effect of  $v_c$  on  $d_{32}$  becomes smaller as the reciprocating of the plates is induced. If  $v_c$  goes up to 8 L/h, the effect of the reciprocating motion is not as significant as the lower  $v_d$  condition.

### 3.1.2. Effect of Reciprocating Frequency

The drop size as a function of the reciprocating frequency is depicted in Figure 8. As the reciprocating frequency increases, the Sauter average droplet diameter,  $d_{32}$ , tends to decrease rapidly. This also can be seen from the photos in Figure 9. When the dispersed phase flow rate is constant, for the continuous phase flow rate, the smaller the continuous phase flow rate, the greater the influence of the reciprocating frequency on the Sauter average droplet diameter,  $d_{32}$ . The reason for this phenomenon may be that the ratio of dispersed phase flow rate to continuous phase flow rate has an effect on the Sauter average droplet diameter,  $d_{32}$  [24].

When the ratio of the dispersed phase flow rate to the continuous phase flow rate is larger, the droplet diameter decreases rapidly under reciprocating vibration condition. When the ratio of the dispersed phase flow rate to the continuous phase flow rate becomes smaller, the influence of the reciprocating vibration becomes smaller, and the influence of the dispersed phase flow rate on the Sauter average droplet diameter,  $d_{32}$ , becomes smaller. The effect of reciprocating frequency is more pronounced in lower-frequency ( $f$ ) and lower-velocity (both  $v_c$  and  $v_d$ ) conditions. Under the reciprocating condition of  $f = 2$  times/min and  $v_c = 2$  L/h, the  $d_{32}$  can reach lower than 10 mm, thus requiring a much lower velocity than the non-reciprocating condition.

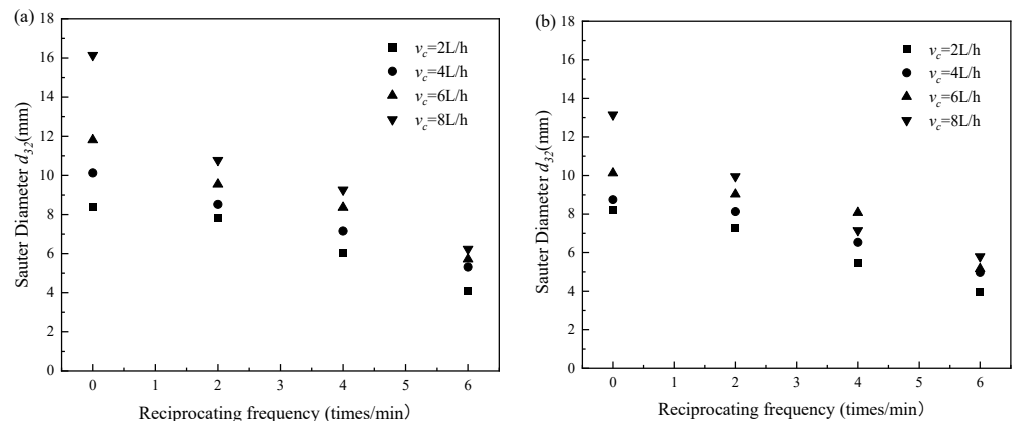


Figure 8. Drop size distribution: (a)  $v_d = 6$  L/h and (b)  $v_d = 9$  L/h.



Figure 9. Drop size distribution of different reciprocating frequency: (a) 2 times/min, (b) 4 times/min, and (c) 6 times/min.

### 3.2. Dispersed Phase Holdup

#### 3.2.1. Effect of Flow Velocity

The dispersed phase holdup can be affected by both flow velocity and frequency. Figure 10 shows the dispersed phase holdup of different dispersed phase velocity. When the dispersed phase velocity is the same, the dispersed phase holdup increases with the increase in the continuous phase velocity. However, the continuous phase flow rate has little effect on the dispersed phase holdup, especially when there is no reciprocating vibration, and the two-phase density difference is countercurrent.

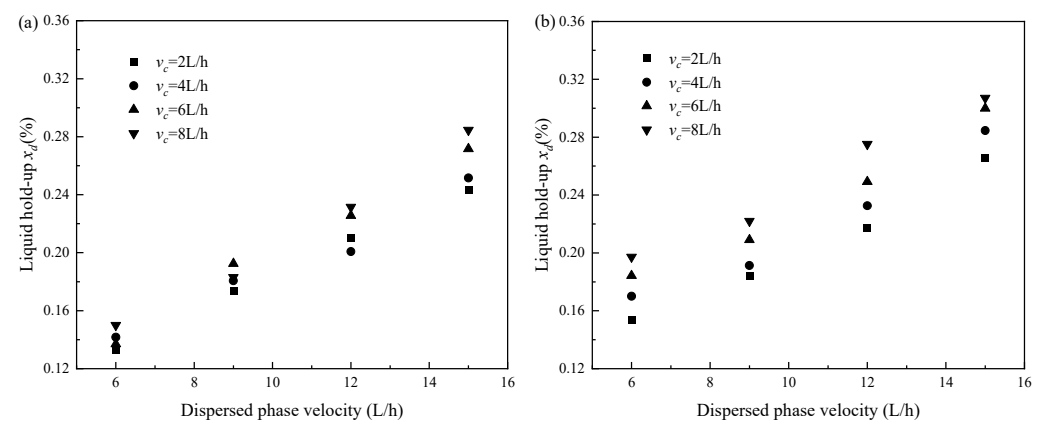


Figure 10. Dispersed phase holdup: (a) stable and (b) reciprocating.

At this time, when the dispersed phase flow rate is small, the dispersed phase holdup fraction under different continuous phase flow rates is very close. When the dispersed phase flow rate increases, the influence of the continuous phase flow rate on the dispersed phase holdup gradually increases. On the whole, the dispersed phase holdup increases significantly with the increase in the dispersed phase velocity. In addition, with the increase in the reciprocating frequency, the dispersed phase retention fraction in the system increases,

because the higher frequency creates more opportunities for the droplets of the dispersed phase to break into smaller sizes. These small droplets rise slowly and stay in the column for a long time, thereby increasing the amount of liquid retention.

### 3.2.2. Effect of Reciprocating Frequency

The reciprocating frequency has a significant effect on the dispersed phase holdup. Figure 11 depicts the dispersed phase holdup as a function of reciprocating frequency. As the reciprocating frequency increases, the dispersed phase holdup increases significantly; it can be clearly seen from Figure 11. The flow rate of the dispersed phase has a significant effect on the dispersed phase holdup caused by the reciprocating frequency. The increase in the flow rate of dispersed phase directly leads to the increase in the retention fraction of the dispersed phase. At higher vibration frequencies, the continuous phase flow rate also has a significant effect on the retention fraction of the dispersed phase. The impact of the reciprocating frequency on the dispersed phase holdup is almost independent of the velocity of the two phases.

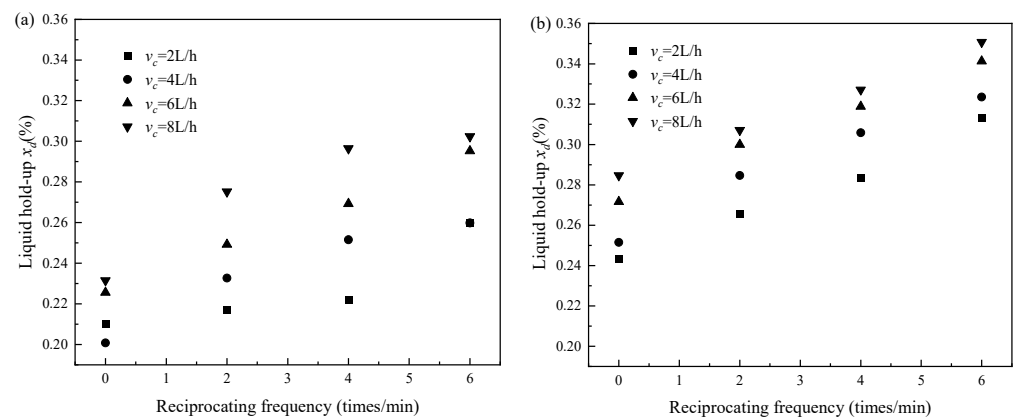


**Figure 11.** Dispersed phase holdup as function of reciprocating frequency: (a)  $v_c = 12$  L/h and (b)  $v_c = 15$  L/h.

### 3.3. Axial Mixing

According to the measurement and calculation methods mentioned in Section 2.4 (c), the RTD (Residence Time Distribution) curve and the axial mixing coefficient,  $E_c$ , of the continuous phase under different conditions were obtained, and the effects of the vibration frequency and two-phase flow rate on the axial mixing of the continuous phase were investigated. The amplitude used in the experiment was 10 mm.

#### 3.3.1. Effect of Reciprocating Frequency

The variation in the RTD curve and axial mixing coefficient,  $E_c$ , of continuous phase was discussed by changing the pulse reciprocating frequency. As shown in Figure 12a, as the reciprocating frequency increases, the peak value of the RTD curve decreases. At the same time, the time for the RTD curve to reach the peak is slightly reduced. It can be seen from Figure 12b that with the increase in the vibration frequency, it shows an increasing trend. This is because the reciprocating motion of the sieve plate increases the turbulence of the fluid in the column.

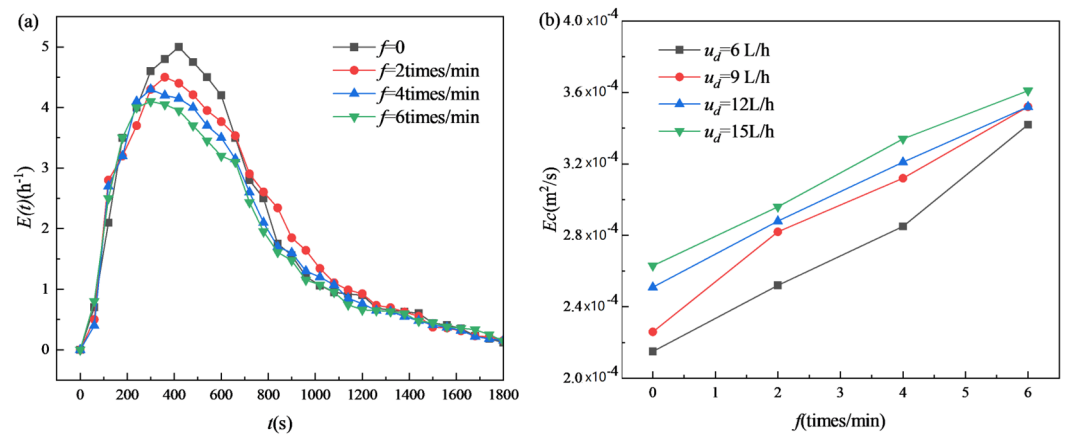


**Figure 12.** Effects of reciprocating frequency on RTD curves and axial dispersion coefficient: (a) RTD curve and (b) axial dispersion coefficient.

### 3.3.2. Effect of Continuous Phase

The effect of continuous phase flow rate on axial mixing was studied when the dispersed phase flow rate was 2 L/h and the reciprocating frequency was 2 times/min. The results are shown in Figure 13. With the increase in the continuous phase flow rate, the peak value of the RTD curve increases obviously, and the time to reach the peak value is relatively close. The axial mixing coefficient increases significantly with the increase in the continuous phase flow rate, which is approximately linear with the continuous phase flow rate. In addition, the increasing trend is similar in all the  $v_d$  cases.

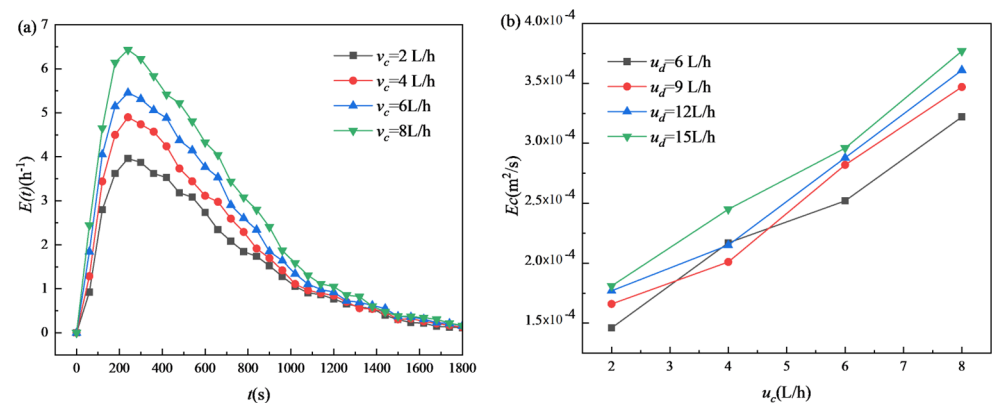


**Figure 13.** Effects of continuous phase velocity on RTD curves and axial dispersion coefficient ( $v_d = 2$  L/h,  $f = 2$  times/min): (a) RTD curve and (b) axial dispersion coefficient.

### 3.3.3. Effect of Dispersed Phase Velocity on Axial Mixing

The effect of dispersed phase flow rate on axial mixing was investigated at a fixed reciprocating frequency of 2 times /min. It can be seen from Figure 14 that the dispersed phase flow rate has little effect on the RTD curve, and the RTD curves under different dispersed phase flow rates are very close, so the influence of the dispersed phase flow rate on the RTD curve can be ignored. As is shown in Figure 14, the influence of the dispersed phase flow rate on the axial mixing coefficient,  $E_c$ , is also very small. In general, the axial mixing coefficient,  $E_c$ , increases with the increase in the dispersed phase flow rate, but the influence of the dispersed phase flow rate on the axial mixing coefficient,  $E_c$ , is negligible compared with the influence of the continuous phase flow rate on the axial mixing coefficient,  $E_c$ .

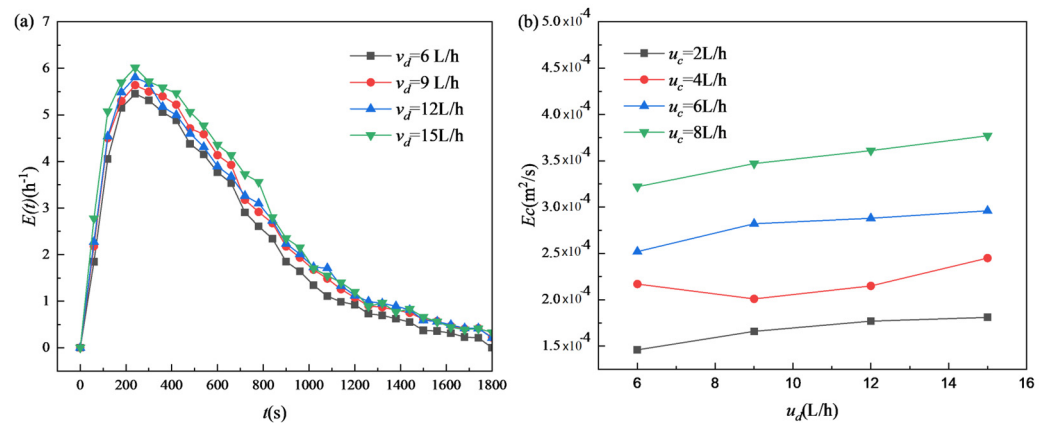


**Figure 14.** Effects of dispersed phase velocity on RTD curves and axial dispersion coefficient ( $v_c = 6$  L/h,  $f = 2$  times/min): (a) RTD curve and (b) axial dispersion coefficient.

#### 4. Discussion

The feasibility of using an electro-permanent magnet truck as the driving device of the reciprocating plate column was verified via a numerical simulation and experiment. In order to further illustrate the advantages of using an electro-permanent magnet truck as the driving device of reciprocating plate column, the experimental conditions and the maximum magnetic field are taken as examples to quantitatively analyze the energy-saving effect.

The maximum current of the permanent magnet sucker used in the experiment is 16 A, the demagnetization current is 10 A, and the time required for magnetization and demagnetization is 20 ms. In the experiment of reciprocating plate column, it usually takes dozens of minutes to run, so the experiment time is 30 min, and the frequency of the reciprocating plate column based on electro-permanent magnet technology is six times per minute.

The traditional geared motor, according to the formula of electric power consumption of energy, is the product of power and time:

$$W = Pt \quad (12)$$

Taking the geared motor with a power of 180 w as an example, the energy consumed in 30 min is 324 kJ. When the electro-permanent magnet truck is used as the driving device, its resistance is 4.4  $\Omega$ . Once the reciprocation is completed, it is necessary to charge and demagnetize each time, and the current consumption energy can be calculated by the following formula:

$$W_{EPM} = (I_m^2 + I_d^2)Rt \quad (13)$$

As is shown in Table 5, the energy consumed by the electro-permanent magnet chuck for 30 min is 4.7 kJ. It can be seen that, in the long-term operation, the energy consumption of the electric permanent magnet chuck as the driving device of the reciprocating plate column is only 1.45% of that of the traditional geared motor as the driving device, and the electro-permanent magnet chuck has great advantages in energy consumption. As the price of the EPM device is a little higher than the motor, the cost margin can still be covered in 2 years by saving energy. Considering a 10-year service life for this kind of device, the device has a comprehensive economic and environmental benefits.

**Table 5.** Energy consumption analysis of two riving devices.

| Name         | Parameters               | Woking Time | Energy Consumption |
|--------------|--------------------------|-------------|--------------------|
| Geared motor | 180 w                    | 30 min      | 324 kJ             |
| EPM chuck    | 16 A, 10 A, 4.4 $\Omega$ | 30 min      | 4.7 kJ             |

## 5. Conclusions

In this paper, a new type of reciprocating plate column based on electro-permanent magnet technology was proposed to realize higher efficiency and energy conversation. The feasibility of this new type of reciprocating plate column was verified via experiments.

With the increase in the dispersed phase flow rate, the Sauter mean diameter ( $d_{32}$ ) decreases, but with the increase in the vibration frequency, the influence of the dispersed phase flow rate on the Sauter mean diameter ( $d_{32}$ ) gradually decreases. The continuous phase flow rate has little effect on the dispersed phase holdup, which is greatly affected by the dispersed phase flow rate and vibration frequency. The dispersed phase holdup increases with the increase in the dispersed phase flow rate and the increase in the vibration frequency. The reciprocating frequency and continuous phase flow rate have a great influence on the axial mixing coefficient of the continuous phase, and the dispersed phase flow rate has little effect on the axial mixing coefficient of the continuous phase.

A quantitative energy consumption analysis of the traditional reciprocating plate column with a geared motor and the reciprocating plate column driven by electro-permanent magnet chuck was carried out. The results show that the energy saving of the reciprocating plate column with an electro-permanent magnet chuck is 98.55%. The performance can be controlled by the reciprocating frequency and flow velocities, which is promising in high-efficiency unit process equipment.

**Author Contributions:** Conceptualization, H.Z.; methodology, J.J.; software, J.J.; validation, D.Z.; formal analysis, J.J.; investigation, Y.Z.; data curation, L.M.; writing—original draft preparation, K.G.; writing—review and editing, X.F.; funding acquisition, K.G. All authors have read and agreed to the published version of the manuscript.

**Funding:** This work is supported by National Natural Science Foundation of China (22308297) and Science and Technology Project of Hebei Education Department, China (QN2022144).

**Data Availability Statement:** The data presented in this study are available on request from the corresponding author.

**Acknowledgments:** Xiantao Fan would also like to acknowledge the fellowship provided by the Environmental Change Initiative and Center for Sustainable Energy at University of Notre Dame.

**Conflicts of Interest:** The authors declare no conflicts of interest.

## References

1. Zhang, J.; Berry, J.D.; Mumford, K.A.; Harvie, D.J.; Fei, W.; Stevens, G.W.; Wang, Y. Single drop breakage in a reciprocating plate column. *Chem. Eng. J.* **2021**, *415*, 129049. [[CrossRef](#)]
2. Stella, A.; Mensforth, K.H.; Bowser, T. Mass Transfer Performance in Karr Reciprocating Plate Extraction Columns. *Ind. Eng. Chem. Res.* **2008**, *47*, 3996–4007. [[CrossRef](#)]
3. Fei, W. Progresses of study and application on extraction columns. *CIESC J.* **2013**, *64*, 44–51.
4. Stella, A.; Pratt, H.C.; Mensforth, K.H.; Stevens, G.W.; Bowser, T. Backmixing in Karr Reciprocating-Plate Extraction Columns. *Ind. Eng. Chem. Res.* **2006**, *45*, 6555–6562. [[CrossRef](#)]
5. Zhang, J.; Wang, Y.; Fei, W. A states-of-the-art review on research progresses and prospects of liquid-liquid extraction columns. *CIESC J.* **2021**, *72*, 6016–6029.
6. Van Dijck, W. Tower with Internal Perforated Plate Suitable for Extracting Liquids by Treatment with other Liquids and for similar Concurrent Processes. U.S. Patent No. 2011186, 13 August 1935.
7. Karr, A.E. Performance of a Reciprocating Plate Extraction Column. *AIChE J.* **1959**, *5*, 446–452. [[CrossRef](#)]
8. Mohanty, S. Modeling of liquid-liquid extraction column: A review. *Rev. Chem. Eng.* **2000**, *16*, 199–248. [[CrossRef](#)]
9. Smith, K.H.; Bowser, T.; Stevens, G.W. Performance and scale-up of Karr reciprocating plate Extraction Columns. *Ind. Eng. Chem. Res.* **2008**, *47*, 8368–8375. [[CrossRef](#)]
10. Zhang, J.; Li, W.; Mumford, K.A.; Fei, W.; Stevens, G.W.; Wang, Y. Mass transfer study and combined model for a Karr column. *Chem. Eng. Sci.* **2022**, *254*, 117581. [[CrossRef](#)]
11. Baird, M.H.I.; Lane, S.J. Drop size and holdup in a reciprocating plate extraction column. *Chem. Eng. Sci.* **1973**, *28*, 947–957. [[CrossRef](#)]
12. Parthasarathy, P.; Sriniketan, G.; Srinivas, N.S.; Varma, Y.B.G. Axial mixing of continuous phase in reciprocating plate columns. *Chem. Eng. Sci.* **1984**, *39*, 987–995. [[CrossRef](#)]

13. Bensalem, A.; Steiner, L.; Hartland, S. Effect of mass transfer on drop size in a Karr column. *Chem. Eng. Process. Process Intensif.* **1986**, *20*, 129–135. [[CrossRef](#)]
14. Zhang, Y.; Li, L. Study on hoisting and handling steel plate by electromagneto chucks. *J. Mach. Des.* **2002**, *19*, 3–6.
15. Ruiz-Calaforra, A.; Brächer, T.; Lauer, V.; Pirro, P.; Heinz, B.; Geilen, M.; Chumak, A.V.; Conca, A.; Leven, B.; Hillebrands, B. The Role of the Non-Magnetic Material in Spin Pumping and Magnetization Dynamics in NiFe and Co Fe B Multilayer Systems. *J. Appl. Phys.* **2015**, *117*, 10–281. [[CrossRef](#)]
16. Billoni, O.V.; Urreta, S.E.; Fabietti, L.M.; Bertorello, H.R. Dependence of the Coercivity on the Grain Size in a Fe NdB/a+Fe Nanocrystalline Composite with Enhanced Remanence. *J. Magn. Magn. Mater.* **1998**, *187*, 371–380. [[CrossRef](#)]
17. Cullity, B.D.; Graham, C.D. *Introduction to Magnetic Materials*; John Wiley and Sons Inc.: Hoboken, NJ, USA, 2009; pp. 44–85.
18. Yuan, X.; Rong, H.; Zhou, X. Design idea of permanent magnet lifting sucker. *Hoisting Conveying Mach.* **2001**, *7*, 11–13.
19. Zhang, H.S.; Qin, S.J.; Cao, L.Q.; Meng, L.Y.; Cheng, X.; Mao, Y. Deep drawing with radial segmental blank holder based on magnetic control. *Sci. Sin. Technol.* **2021**, *51*, 388–398. (In Chinese) [[CrossRef](#)]
20. Chang, P.; Bao, X. New type of Ship Mooring Device Based on Electronically Controlled Permanent Magnetic Chuck. *Navig. China* **2015**, *38*, 18–21.
21. Chang, X.; Yang, D.; Sun, K. Design and Optimization of Electropermanent Magnet Suckers in Horizontal Well Tractors. *China Mech. Eng.* **2019**, *30*, 1–5.
22. Zhong, Y.; Liu, Y.; Zhang, S. Method Comparison for Determining the Concentration of Benzoic Acid in the Experiment of Water-Kerosene Extraction. *Univ. Chem.* **2019**, *34*, 66–72. [[CrossRef](#)]
23. Wu, Y.; Vovers, J.; Lu, H.T.; Li, W.; Stevens, G.W.; Mumford, K.A. Investigation of the extraction of natural alkaloids in Karr reciprocating plate columns: Fluid dynamic study. *Chem. Eng. Sci.* **2022**, *264*, 118090. [[CrossRef](#)]
24. Jackson, C.S.; Skaf, W.D. Implementing a KARR<sup>®</sup> extraction column in the unit operations lab. *Educ. Chem. Eng.* **2020**, *32*, 95–101. [[CrossRef](#)]

**Disclaimer/Publisher’s Note:** The statements, opinions and data contained in all publications are solely those of the individual author(s) and contributor(s) and not of MDPI and/or the editor(s). MDPI and/or the editor(s) disclaim responsibility for any injury to people or property resulting from any ideas, methods, instructions or products referred to in the content.